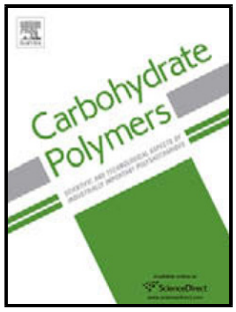

Title: Nanocellulose-based antifungal nanocomposites against the polymorphic fungus *Candida albicans*

Authors: Carla Vilela, Helena Oliveira, Adelaide Almeida, Armando J.D. Silvestre, Carmen S.R. Freire

PII: S0144-8617(19)30439-4
DOI: https://doi.org/10.1016/j.carbpol.2019.04.046
Reference: CARP 14820

To appear in:

Received date: 20 December 2018
Revised date: 8 April 2019
Accepted date: 9 April 2019

Please cite this article as: Vilela C, Oliveira H, Almeida A, Silvestre AJD, Freire CSR, Nanocellulose-based antifungal nanocomposites against the polymorphic fungus *Candida albicans*, *Carbohydrate Polymers* (2019), https://doi.org/10.1016/j.carbpol.2019.04.046

Nanocellulose-based antifungal nanocomposites against the polymorphic fungus *Candida albicans*

Carla Vilela [a,*], Helena Oliveira [b], Adelaide Almeida [b], Armando J. D. Silvestre [a], Carmen S. R. Freire [a]

[a] CICECO – Aveiro Institute of Materials, Department of Chemistry, University of Aveiro, 3810-193 Aveiro, Portugal

[b] Department of Biology and CESAM, University of Aveiro, 3810-193 Aveiro, Portugal

Corresponding author: C. Vilela (cvilela@ua.pt)

Graphical abstract

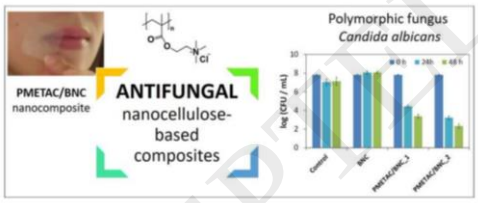

Highlights

- Poly([2-(methacryloyloxy)ethyl]trimethylammonium chloride)/nanocellulose composites.
- Cationic nanocomposites with UV–blocking properties and high water-uptake capacity.

- BNC enhanced the thermal, viscoelastic and mechanical properties of the nanocomposites.
- Bioactive nanocomposites capable of inactivating the polymorphic fungus *Candida albicans*.
- *C. albicans* inactivation of 4.4– and 5.5–log CFU reduction after 24 and 48 hours.

Abstract

The design of functional materials capable of fighting fungal infections is of paramount importance given the intricate problem of multidrug-resistant pathogenic fungi. Herein, nanocomposites consisting of cross-linked poly([2–(methacryloyloxy)ethyl] trimethylammonium chloride) (PMETAC) and bacterial nanocellulose (BNC) were prepared, characterized and tested towards the polymorphic fungus *Candida albicans*. The BNC three-dimensional network enabled the *in-situ* polymerization of the non-toxic and bioactive quaternary-ammonium monomer, which originated transparent nanocomposites containing 10 and 40 wt.% of cross-linked PMETAC. Furthermore, the nanocomposites exhibit UV–A and UV–B blocking properties, high water-uptake capacity, thermal stability up to 200 °C, good viscoelastic (storage modulus > 1.7 GPa) and mechanical (Young's modulus ≥ 2.4 GPa) properties and are non-cytotoxic to human keratinocytes (HaCaT cells). The fungal inactivation reached a 4.4±0.14–log CFU reduction for the nanocomposite containing only 10 wt.% of cross-linked PMETAC. Hence, these bioactive and non-cytotoxic materials can constitute potentially effective systems for the treatment of *C. albicans* infections.

Keywords: antifungal activity; bacterial nanocellulose; *Candida albicans*; cutaneous treatment; *in-situ* polymerization; poly([2–(methacryloyloxy)ethyl]trimethylammonium chloride)

1. Introduction

Fungal infections caused by *Candida albicans* are a major health problem since this microorganism has the potential to cause life-threatening localized and systemic infections (Dadar et al., 2018). *C. albicans* is a polymorphic fungus that, despite being part of the normal human microbiome as a harmless commensal, is also an opportunist pathogen that can cause simple superficial skin and mucosal infections, or escalade into systemic infections depending on the host vulnerability, such as in the case of immunocompromised or immunologically deficient individuals (Dadar et al., 2018; Mayer, Wilson, & Hube, 2013). This major pervasive pathogenic fungus forms architecturally complex biofilms on a variety of host tissues (*e.g.*, skin, mucosal and bed nails), teeth, dentures, catheters, and other biomedical implants (Kühbacher, Burger-Kentischer, & Rupp, 2017; Sheppard & Howell, 2016; Soll & Daniels, 2016), and the extracellular polysaccharide matrix is responsible for their resistance mechanisms (Tsui, Kong, & Jabra-Rizk, 2016). In this sense, the need to engineer antifungal materials that can avoid or reduce the growth of fungus is a research topic worth tackling (Zida, Bamba, Yacouba, Ouedraogo-Traore, & Guiguemdé, 2017).

Naturally occurring polymers, such as polysaccharides and proteins (Silva et al., 2014; Vilela, Pinto, et al., 2018), are becoming important substrates to develop multifunctional materials for antimicrobial applications (Wang & Vermerris, 2016). While some of the biopolymers are natural biocides such as chitosan (Vilela, Pinto, Coelho, et al., 2017) and lysozyme nanofibers (Silva, Vilela, Almeida, Marrucho, &

Freire, 2018), others like cellulose (the most abundant biopolymer on earth) must be combined with bioactive compounds in order to acquire such features (Li et al., 2018). In fact, cellulose is starting to make headway into antimicrobial materials particularly in its nanoscale forms, *viz*. bacterial nanocellulose (BNC), cellulose nanofibrils (CNFs) and cellulose nanocrystals (CNCs) (Li et al., 2018). The former nanometric form, *i.e*. BNC, albeit the absence of biocide properties, presents several bonus characteristics for the development of bioactive materials, namely *in-situ* moldability, shape retention (A. R. P. Figueiredo, Vilela, Neto, Silvestre, & Freire, 2015; Vilela, Pinto, Figueiredo, et al., 2017), three-dimensional morphology control across several length scales (Greca, Lehtonen, Tardy, Guo, & Rojas, 2018), and ability to house different (macro)molecules within its ultrafine nanofibrous network (Cielecka et al., 2018; Faria, Vilela, Mohammadkazemi, et al., 2019; Padrão et al., 2016; Subtaweesin et al., 2018). One of the easiest and versatile approach to fabricate BNC derived nanomaterials is based on the *in-situ* polymerization of functional monomers within the BNC porous network, as reviewed by Ray and Sain (Ray & Sain, 2016). This originates materials with properties that the exopolysaccharide does not have by itself, such as stimuli-responsiveness (Saïdi, Vilela, Oliveira, Silvestre, & Freire, 2017), ionic conductivity (Gadim et al., 2014; Vilela, Martins, et al., 2018), amphoterism (Faria, Vilela, Silvestre, et al., 2019), or antibacterial activity against for example *Escherichia coli* (Figueiredo, Figueiredo, et al., 2015).

[2–(Methacryloyloxy)ethyl]trimethylammonium chloride (METAC) is a functional monomer with a tremendous potential to be used in association with BNC. In fact, the easily polymerizable methacrylic functional group of METAC (Morales, Rivas, & González, 2016; Morales, Rivas, & Escalona, 2016) that leads to the formation of cationic water-soluble polymers and hydrogels (Nurkeeva et al., 2006) together with its

non-toxicity, mucoadhesive properties (Fefelova, Nurkeeva, Mun, & Khutoryanskiy, 2007) and antifungal activity against *C. albicans* (Stopiglia et al., 2012) are the major assets for selecting this monomer to design antifungal materials (Muñoz-Bonilla & Fernández-García, 2018). For example, Stopiglia *et al*. highlighted that METAC monomer exhibits antifungal activity against *C. albicans*, as well as other *Candida* species, with a minimum inhibitory concentration (MIC) of 50 mg mL^{-1} and a minimum fungicidal concentration (MFC) higher than 100 mg mL^{-1} (Stopiglia et al., 2012). According to these authors, METAC can be copolymerized with other methacrylic monomers to fabricate denture acrylic resins or denture temporary soft lining materials, and the presence of this fungal inhibitor will avoid denture-related stomatitis mostly caused by *C. albicans* (Stopiglia et al., 2012). In a different study, De Prijck *et al*. demonstrated that grafting PMEATC onto the surface of a voice prothesis prevented *C. albicans* biofilms formation which is a major cause of voice prosthesis deterioration in laryngectomized patients (De Prijck, De Smet, Coenye, Schacht, & Nelis, 2010).

Albeit the association between BNC and poly([2–(methacryloyloxy)ethyl] trimethylammonium chloride) (PMETAC) was already studied in the context of polyelectrolytic membranes with ionic conductivity for application in fuel cells (Vilela, Sousa, et al., 2017), the behaviour of PMETAC/BNC nanocomposites as antifungal materials against the polymorphic *C. albicans* has not been investigated yet. In fact, the inherent purity, biodegradability, biocompatibility and high water-holding capacity of BNC (Gama, Dourado, & Bielecki, 2017), and the antifungal activity of PMETAC against *C. albicans* (Stopiglia et al., 2012), is an interesting partnership to engineer materials capable of inactivating this opportunistic polymorphic fungus. In this perspective, the present study aims at developing nanocomposite materials consisting of cross-linked PMETAC and BNC via the *in-situ* free radical polymerization of the

bioactive quaternary ammonium monomer within the BNC porous structure. The systematic characterization of the PMETAC/BNC nanocomposites with different PMETAC and BNC contents was performed in terms of structure, morphology, optical properties, water-uptake capacity, thermal stability, mechanical and viscoelastic properties, antifungal activity against *C. albicans* and cytotoxicity against human keratinocytes (HaCaT cells).

2. Experimental

2.1. Chemicals, materials and microorganisms

[2–(Methacryloyloxy)ethyl] trimethylammonium chloride solution (METAC, 75 wt.% in H_2O, Aldrich), 2,2′–azobis(2–methylpropionamidine) dihydrochloride (AAPH, 97%, Aldrich) and *N*,*N*′–methylenebis(acrylamide) (MBA, 99%, Sigma-Aldrich) were used as received. Other chemicals and solvents were of laboratory grade. Bacterial nanocellulose (BNC) wet pellicles were biosynthesized in our research laboratory using the *Gluconacetobacter sacchari* bacterial strain (Trovatti, Serafim, Freire, Silvestre, & Neto, 2011). *Candida albicans* (SC5314) was provided by DSMZ – Deutsche Sammlung von Mikroorganismen und Zellkulturen GmbH (German Collection of Microorganisms and Cell Cultures).

The nontumorigenic immortalized human keratinocyte HaCaT cell line was obtained from Cell Lines Services (Eppelheim, Germany), phosphate buffer saline (PBS, pH 7.4), Dulbecco′s Modified Eagle′s Medium (DMEM), fetal bovine serum (FBS), L-glutamine, penicillin/streptomycin and fungizone were supplied by Gibco® (Life Technologies, Carlsbad, CA, USA), and 3-(4,5-dimethylthiazolyl-2)-2,5-diphenyltetrazolium bromide (MTT, 98%) was purchased from Sigma-Aldrich.

2.2. PMETAC/BNC nanocomposites

Wet BNC pellicles (diameter: *ca*. 7 cm) with 40% water content were placed in stoppered glass-reactors and purged with nitrogen. Simultaneously, aqueous solutions of METAC (1:1.5 and 1:5 BNC/METAC weight fraction), AAPH (1%, w/w relative to monomer) and MBA (5%, w/w relative to monomer) were prepared and transferred to the glass-reactors containing the drained BNC pellicles. After the complete incorporation of the corresponding solution during 1 h in ice, the reaction mixtures were heated in an oil bath at 70 °C during 6 h. Afterwards, the nanocomposites were

repeatedly washed with water, oven dried at 40 °C for 24 h, and kept in a desiccator until further use. All experiments were made in triplicate and samples of cross-linked PMETAC were also prepared in the absence of BNC.

2.3. Characterization methods

Thickness: a hand-held digital micrometer (Mitutoyo Corporation, Japan) with an accuracy of 0.001 mm was used to measure the thickness of the materials. All measurements were randomly performed at different sites of the samples.

Elemental analysis: the elemental composition was determined by elemental analysis using a LECO TruSpec 630-200-200 CHNS elemental analyser (LECO Corporation, USA) with a combustion furnace and afterburner temperatures of 1075 °C and 850 °C, respectively. All samples (*ca*. 5 mg) were analysed in triplicate.

Attenuated total reflection-Fourier transform Infrared (ATR–FTIR): ATR-FTIR spectra were recorded with a Perkin-Elmer FT–IR System Spectrum BX spectrophotometer (Perkin-Elmer Inc., USA) equipped with a single horizontal Golden Gate ATR cell, over the range of 600–4000 cm^{-1} at a resolution of 4 cm^{-1} over 32 scans.

Solid-state carbon cross-polarization/magic-angle-spinning nuclear magnetic resonance (^{13}C CP/MAS NMR): ^{13}C CP/MAS NMR spectra were collected on a Bruker Avance III 400 spectrometer (Bruker Corporation, USA) operating at a B0 field of 9.4 T using 9 kHz MAS with proton 90° pulse of 3 μs, time between scans of 3 s, and a contact time of 2000 μs. ^{13}C chemical shifts were referenced to glycine (C=O at δ 176 ppm).

X-ray diffraction (XRD): XRD was performed on a Phillips X'pert MPD diffractometer (PANalytical, Netherlands) using Cu Kα radiation (λ = 1.541 Å) with a

scan rate of 0.05° s^{-1}. The XRD patterns were collected in reflection mode with the samples placed on a Si wafer (negligible background signal) for mechanical support and thus avoid sample bending.

Scanning electron microscopy (SEM): SEM images of the surface and cross-section of the samples were obtained by a HR-FESEM SU–70 Hitachi microscope (Hitachi High-Technologies Corporation, Japan) operating at 4 kV. The samples were previously coated with a carbon film.

Ultraviolet-visible spectroscopy (UV–vis): the transmittance spectra of the samples were acquired with a Shimadzu UV-1800 UV-Vis spectrophotometer (Shimadzu Corp., Japan) equipped with a quartz window plate with 10 mm diameter, bearing the holder in the vertical position. Spectra were recorded at room temperature in steps of 1 nm in the range 250–700 nm.

Water-uptake capacity (*WU*): the *WU* was determined via immersion of dry specimens with 10×10 mm^2 in distilled water at room temperature (RT) during 120 h. After removing the specimens out of the water, the wet surfaces were dried in filter paper, and the wet weight (W_w) was measured. The *WU* is calculated by the equation: $WU\ (\%) = [(W_w - W_0)/W_0]$, where W_0 is the initial weight of the dry sample. At the end of the immersion tests in water (120 h), the nanocomposite specimens were oven dried at 40 °C during 24 h in a vacuum drying oven (Thermo Fisher Scientific, USA) and their dry weight measured to determine the leaching of cross-linked PMETAC. All samples were analysed in triplicate.

Thermogravimetric analysis (TGA): TGA was carried out with a SETSYS Setaram TGA analyser (SETARAM Instrumentation, France) equipped with a platinum cell. The samples were heated from RT to 800 °C at a constant rate of 10 °C min^{-1} under a nitrogen atmosphere (200 mL min^{-1}).

Tensile tests: tensile tests were performed on a uniaxial Instron 5564 testing machine (Instron Corporation, USA) in the traction mode at a cross-head velocity of 10 mm min^{-1} using a 500 N static load cell. The specimens were rectangular strips (50×10 mm^2) previously dried at 40 °C and equilibrated at RT in a 50% relative humidity (RH) atmosphere prior to testing. All measurements were performed on five replicates.

Dynamic mechanical analysis (DMA): DMA curves of rectangular specimens with 30×5 mm^2 were obtained on a Tritec 2000 DMA (Triton Technologies Ltd., UK) operating in tension mode (single strain) at 1 Hz and with 0.005 mm displacement. The temperature was sweep from −30 to 180 °C with a constant heating rate of 2 °C min^{-1}. Before the measurements, the samples were kept in a conditioning cabinet at 30 °C and 50% relative humidity (RH) for 48 h.

2.4. In vitro antifungal activity

The antifungal activity of the nanocomposites was tested against *C. albicans* (SC5314). All fungal pre-inoculum cultures were grown overnight at 37 °C in 50 mL Yeast Glucose Chloramphenicol (YGC: 20 g L^{-1} D-glucose, 5 g L^{-1} yeast extract and 0.1 g L^{-1} chloramphenicol; Liofilchem®, Italy) broth, under shaking of 100 rpm.

For all nanocomposites, 50 mg of each material was placed in contact with 10 mL of a liquid yeast suspension, prepared by ten-fold diluting the overnight grown culture in YGC. Control yeast cell suspension and control cellulose samples were also run in each antifungal test. All samples were incubated at 37 °C. At time 0 and after 12, 24, 36 and 48 h of incubation, aliquots (500 µL) of each sample and controls were collected and the yeast cell concentration (CFU mL^{-1}) was determined by plating serial dilutions on YGC Agar (YGC: 20 g L^{-1} D-glucose, 5 g L^{-1} yeast extract, 0.1 g L^{-1}

chloramphenicol and 18 g L^{-1} agar; Liofilchem®, Italy). Three independent experiments were carried out.

Statistical analysis was performed using GraphPad Software (GraphPad Prism 6, GraphPad Software Inc., La Jolla, CA, USA). The existence of significant differences among the different samples tested was assessed by one-way ANOVA. For each situation, the significance of differences was evaluated by comparing the results obtained in the test samples with the result obtained for the corresponding control samples (difference between the concentration obtained in the control and the concentration obtained in the test sample), as well as the differences obtained between samples, for the different times of each of the three independent assays. A value of $p<0.05$ was considered significant.

2.5. In vitro cytotoxicity assays

The cytotoxicity of the nanocomposites was evaluated in human keratinocyte cell line (HaCaT cells) by using the MTT assay (Mosmann, 1983). Briefly, cells were grown in complete DMEM supplemented with 10% FBS, 2 mM L-glutamine, 10000 U mL^{-1} penicillin/streptomycin and 250 µg mL^{-1} fungizone at 37 °C in 5% CO_2 humidified atmosphere. Cells were daily observed under an inverted phase-contrast Eclipse TS100 microscope (Nikon, Tokyo, Japan). The tests were performed in triplicates of pure BNC and nanocomposites PMETAC/BNC_1 and PMETAC/BNC_2. As a negative control, HaCaT cells were treated identically as described for the samples and no positive control was tested. Samples of 1×1 cm^2 were prepared, rinsed with ultra-pure water, sterilized in ethanol for 1 h, rinsed several times with sterilize PBS to completely remove the ethanol, and then incubated with 1.5 mL of complete DMEM medium at 37 °C, with 5% CO_2 for 24 h to prepare the extract.

In the meantime, one 96 wells plate was prepared with 5×4 wells filled up with 6000 cells/well and the cells were then incubated in complete culture medium during 24 h for adhesion. After that time, cell culture medium (in the 96 well plates) was replaced by 100 µL of each of the extracts obtained from the incubated samples and cells were then further incubated for 24 h.

At the end of the incubation time, 50 µL of MTT (at a concentration of 1 g L^{-1}) were added to each well and incubated for 4 h at 37 °C in 5% CO_2 humidified atmosphere. After that, culture medium with MTT was removed and replaced by 150 µL of dimethyl sulfoxide (DMSO) and the plate was placed in a shaker for 2 h in the dark to completely dissolve the formazan crystals. The absorbance of the samples was measured with a BioTek Synergy HT plate reader (Synergy HT Multi-Mode, BioTeK, Winooski, VT) at 570 nm with blank corrections. Data was analysed by a two-way ANOVA followed by a Holm-Šídák test to determine the significance between the two nanocomposites.

3. Results and discussion

The exopolysaccharide BNC can house all kinds of molecules from bioactive compounds (*e.g.* curcumin (Subtaweesin et al., 2018)) to monomers and polymers (*e.g.*, lactoferrin (Padrão et al., 2016) and κ-carrageenan (Cielecka et al., 2018)) with the purpose of developing nanocomposite and hybrid materials with distinct properties. Therefore, the *in-situ* free radical polymerization of the cationic METAC within the swollen BNC network was used to prepare two PMETAC/BNC nanocomposites. The reaction scheme of the METAC polymerization in the presence of MBA as cross-linker and using water as solvent, is outlined in Fig. 1A. The MBA cross-linker (Shiga et al., 2018) was used with aim of retaining the bioactive quaternary ammonium-based

polymer inside the BNC porous structure, since the non-cross-linked amphiphilic PMETAC is water soluble (Fefelova et al., 2007; Nurkeeva et al., 2006), and would leach out upon contact with aqueous media (*e.g.*, during the washing steps of the nanocomposite preparation), as indeed shown for other water soluble polymers (Figueiredo, Figueiredo, et al., 2015).

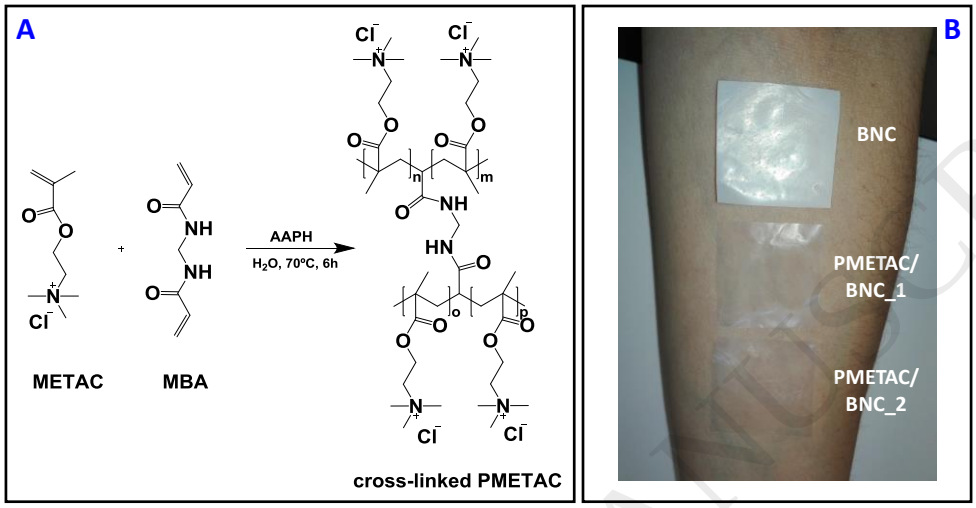

Fig. 1. (A) Radical polymerization of METAC in the presence of MBA as cross-linker, and (B) photographs showing the visual aspect of a dry BNC, and PMETAC/BNC_1 and PMETAC/BNC_2 nanocomposites placed in the arm.

The thickness of the prepared nanocomposites increased from 45±10 µm for the pristine BNC to 61±10 µm and 118±15 µm for PMETAC/BNC_1 and PMPC/BNC_2, respectively (Table 1). The visual examination of the nanocomposites shows no evident heterogeneities on the bottom and top surfaces, demonstrating a good dispersion of the cross-linked PMETAC inside the BNC porous network, as shown in Fig. 1B. Moreover, the two nanocomposites are more transparent than the white BNC (Fig. 1B, see section 3.2 for further details) and readily absorb moisture from the surrounding due to the hygroscopic nature of PMETAC (Goel et al., 2009). These two features are important in

the context of skin regeneration, namely for visual control of the wound healing process and absorption of exudates, respectively.

The nanocomposites present compositions of 60 or 90 wt.% for BNC (W_{BNC}/W_{total}), and 40 or 10 wt.% for PMETAC (W_{PMETAC}/W_{total}), which translates into materials containing 209±9 or 570±12 mg of PMETAC *per* cm^3 of nanocomposite, respectively, as summarized in Table 1. This was further corroborated by elemental analysis with the following compositions: (i) *C*: 41.4±0.5%, *H*: 6.7±0.3%, *O*: 49.2±0.9% and *N*: 2.7±0.1% for PMETAC/BNC_1, and (ii) *C*: 41.9±0.2%, *H*: 6.6±0.1%, *O*: 46.8±0.1% and *N*: 4.7±0.3% for PMETAC/BNC_2, where, as expected, the latter nanocomposite presents a higher nitrogen content.

Table 1 Weight composition and thickness of the PMETAC/BNC nanocomposites.

Samples	Composition			Thickness
	W_{BNC}/W_{total}	W_{PMETAC}/W_{total}	W_{PMETAC}/V_{total} (mg cm^{-3}) [a]	/μm
BNC	1.00	0.00	–	45±10
PMETAC/BNC_1	0.90±0.2	0.10±0.2	209±9	61±10
PMETAC/BNC_2	0.60±0.1	0.40±0.1	570±12	118±15

[a] The composition was calculated by considering the weight of the nanocomposite (W_{total}), BNC (W_{BNC}) and PMETAC (W_{PMETAC}), and also the volume of the nanocomposite (V_{total}); all values are the mean of at least three replicates with the respective standard deviations.

The two PMETAC/BNC nanocomposites (and pure BNC and cross-linked PMETAC for comparison purposes) were characterized regarding their structure (ATR–FTIR, solid-state ^{13}C CP/MAS NMR, XRD), morphology (SEM), optical properties

(UV–vis), water-uptake capacity, thermal stability (TGA), mechanical performance (tensile tests), viscoelastic properties (DMA), antifungal activity (against *C. albicans*) and cytotoxicity (towards HaCaT cells), as discussed in the following sections.

3.1. Structure and morphology

The structural characterization of the two nanocomposites and the corresponding individual components was performed by ATR–FTIR, ^{13}C CP/MAS NMR and XRD, which allowed to confirm the effective inclusion of PMETAC into the BNC three-dimensional porous network. The ATR–FTIR spectra of both PMETAC/BNC nanocomposites (Fig. 2A) combine the absorption bands of both the cross-linked PMETAC and BNC (Fig. S1) at about 3200–3400 cm^{-1} (O–H stretching), 2900 cm^{-1} (C–H stretching), 1720 cm^{-1} (C=O stretching), 1480 cm^{-1} ($N^+(CH_3)_3$ bending), and 951 cm^{-1} ($N^+(CH_3)_3$ stretching) (Bellamy, 1975; Vilela, Sousa, et al., 2017). Moreover, the differences in the intensities of the bands allocated to the cross-linked PMETAC confirm the different contents of the bioactive quaternary ammonium-based polymer inside the BNC network (Table 1).

The solid-state ^{13}C CP/MAS NMR spectra shown in Fig. 2B also validated the composition of the nanocomposites through the presence of the typical carbon resonances of PMETAC (Fig. S1) at δ 19.0 ppm (CH_3 of polymer backbone), 45.2 ppm (quaternary *C* of polymer backbone), 54.4 ppm ($N^+(CH_3)_3$ and CH_2 of polymer backbone), 59.3 ppm (OCH_2), 65.0 ppm ($CH_2N^+(CH_3)_3$) and 177.9 ppm (*C*=O), and of BNC (Fig. S1) at δ 65.2 ppm (C6), 71.4–74.3 ppm (C2,3,5), 90.0 ppm (C4) and 104.8 ppm (C1) (Vilela, Sousa, et al., 2017). The different intensities of the carbon resonances assigned to the cross-linked PMETAC also corroborate the different contents of the PMETAC in the nanocomposites (Table 1).

The XRD patterns (Fig. S2) of the nanocomposites mostly preserved the semi-crystalline nature of BNC with the well-known sharp diffraction peaks at about 2θ 14.3°, 15.9° and 22.6°, instead of the amorphous character of the cross-linked PMETAC (Qi et al., 2017).

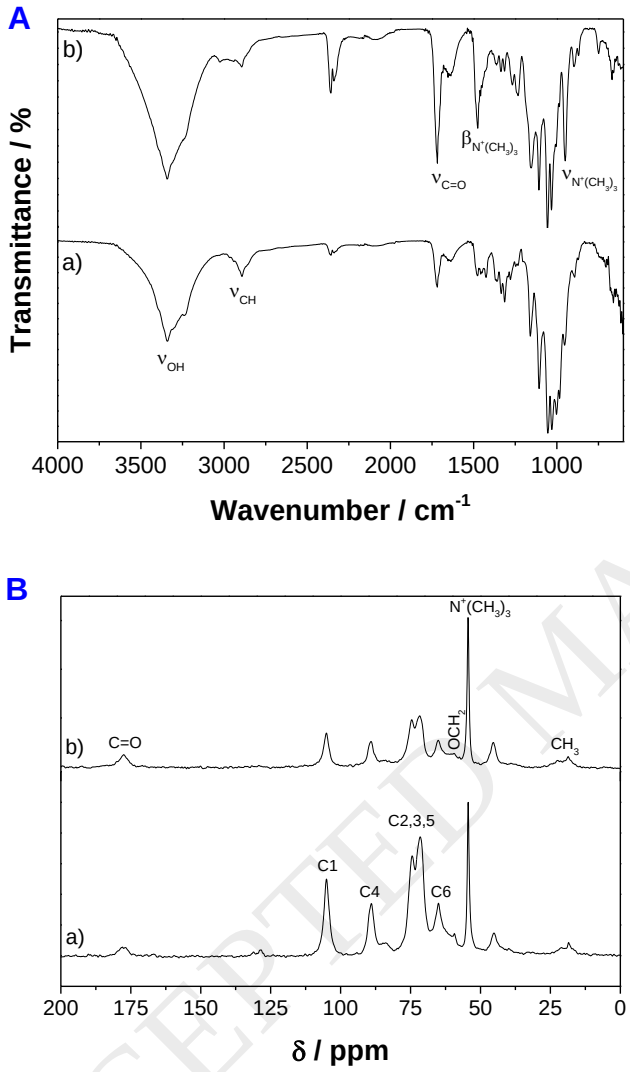

Fig. 2. (A) ATR-FTIR (modes: ν = stretching, β = bending) and (B) ^{13}C CP/MAS NMR spectra of a) PMETAC/BNC_1 and b) PMETAC/BNC_2 nanocomposites.

Concerning the morphology, Fig. 3 displays the SEM micrographs of the surface and cross-section of the two PMETAC/BNC nanocomposites, where it is possible to observe the three-dimensional nanofibrillar network and lamellar microstructural

features of the BNC morphology. As expected, PMETAC/BNC_ 1 is the nanocomposite with the morphology that mostly resembles that of pure BNC because it contains 90 wt.% of BNC, *i.e*. only 209±9 mg of PMETAC *per* cm^3 of nanocomposite (Table 1). On the other hand, the cross-section micrographs of PMETAC/BNC_2 with 60 wt.% of BNC show the filling of the lamellar spaces of the bacterial polysaccharide by the cross-linked cationic PMETAC with 570±12 mg of PMETAC *per* cm^3 of nanocomposite. These micrographs demonstrate the anisotropic morphology of the nanocomposites due to the presence of BNC, along with the homogeneous distribution of the cross-linked PMETAC inside the BNC nanofibrous network.

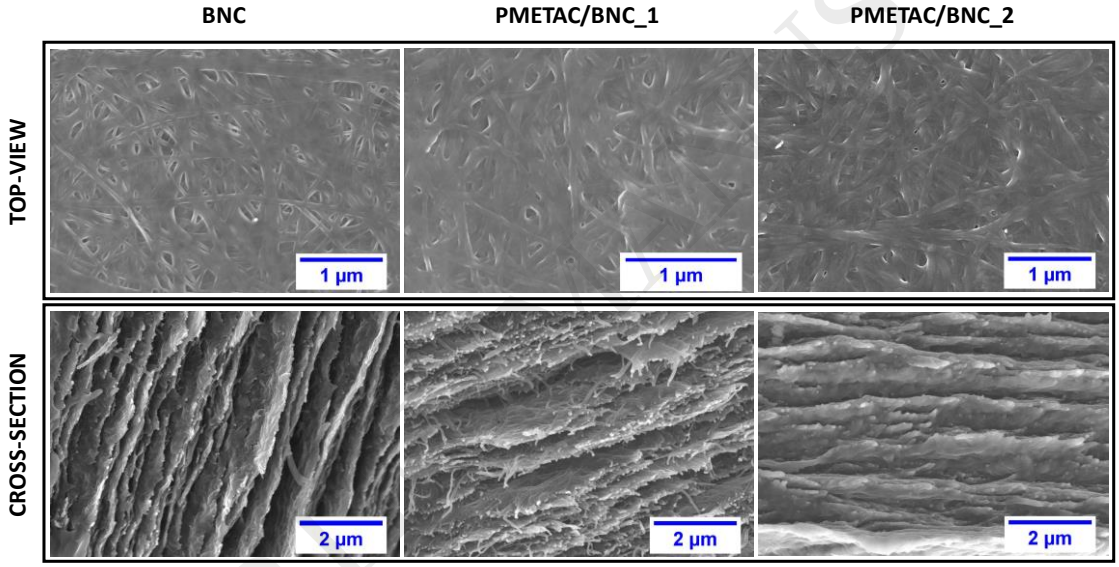

Fig. 3. SEM micrographs of the surface and cross-section of the pure BNC and PMETAC/BNC nanocomposites.

3.2. Optical properties

The optical properties of the pristine BNC and PMETAC/BNC nanocomposites were assessed by measuring the transmittance in the range 250–700 nm. According to Fig. 4, the transmittance of pure BNC only increases in the visible range (400–700 nm) and attains a maximum of *ca*. 8.0% at 700 nm, which demonstrates a low transparency

in tune with its whitish colour (Fig. 1B). The inclusion of cross-linked PMETAC in the BNC porous network originated nanocomposites with higher transparency that increases over the entire visible range of wavelengths, reaching a maximum of about 33% for PMETAC/BNC_1 and 42% for PMETAC/BNC_2 at 700 nm. Furthermore, the transparency augment with the increase of PMETAC content is also observable by the visual examination of the nanocomposites, as illustrated in Fig. 1B. The rationale behind the higher transparency of the nanocomposites when compared to pure BNC might be explained by the overlapping of the optical properties of both the bioactive cross-linked PMETAC and the three-dimensional network assembly of the BNC nanofibers, as discussed elsewhere (Pinto et al., 2015).

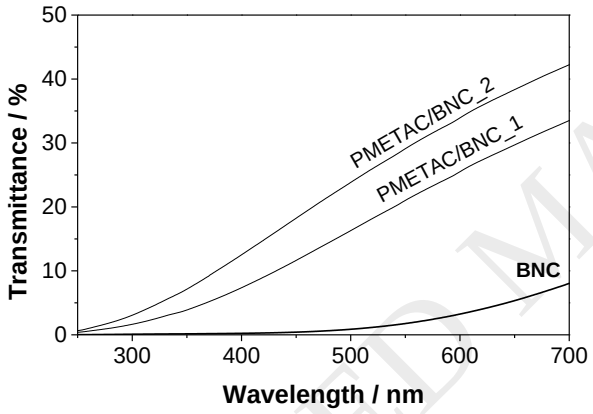

Fig. 4. UV–visible transmission spectra of pure BNC and PMETAC/BNC nanocomposites.

Worth noting is also the fact that the nanocomposites, just like BNC, exhibit notable UV-absorbing properties in both UV–B (280–320 nm, short-wavelength radiation) and UV–A (320–400 nm, long-wavelength radiation) regions. The nanocomposite with the lower PMETAC content (PMETAC/BNC_1, 10 wt.%) presents a transmittance of about 1.0% at 280 nm, 2.5% at 320 nm and 7.4% at 400 nm, whereas the nanocomposite with the higher PMEATC content (PMETAC/BNC_2, 40 wt.%)

shows a transmittance of *ca*. 1.9% at 280 nm, 4.6% at 320 nm and 12.5% at 400 nm. These UV-blocking properties are quite interesting for cutaneous infected wounds that worsen from exposure to UV radiation (UV-induced damage) either from sunlight or artificial light sources (Gupta, Avci, Dai, Huang, & Hamblin, 2013).

3.3. Water-uptake capacity

The water-uptake (*WU*) is an important property to assess the performance of the PMETAC/BNC nanocomposites. In fact, the *WU* of the biocompatible BNC is a relevant characteristic of this exopolysaccharide that allows it to absorb exudates when adhered to the skin surface (Silvestre, Freire, & Neto, 2014). According to Fig. 5, BNC absorbed water during the experiments with a *WU* pattern consisting of two different regions: in the first hours the absorption was fast (*WU* = 62.5±7% after 3 h) and then an equilibrium plateau was steadily reached (*WU* = 100±9% after 48 h).

The two nanocomposites absorbed water with similar profiles composed of two different regions but with distinct values. While PMETAC/BNC_1 containing 209 mg PMETAC *per* cm^3 of nanocomposite shows a *WU* of 225±19% after 48 h of immersion in water, the nanocomposite with higher content of cross-linked PMETAC (40 wt.%) exhibited the higher *WU* value 873±56% (Fig. 5, $p<0.05$). As expected, these high *WU* values come with the increase of nanocomposite dimensions. This behaviour is in accordance with the very hygroscopic nature of tetraalkylammonium salts (Goel et al., 2009). Analogous values were reported in literature (Vilela, Sousa, et al., 2017), including for a METAC–grafted cotton fabric (~18% grafting) that reached a *WU* value of *ca*. 500% compared to the *WU* of *ca*. 150% of the pure cotton cellulose fibres present in the fabric (Goel et al., 2009). The fact that the PMETAC/BNC nanocomposites

absorb considerable amounts of water is relevant in the context of infections that originate exudates such as pus-like or clear fluids.

The samples from the *WU* tests were also used to determine the possible leaching of cross-linked PMETAC from the nanocomposites. After 120 h of immersion in water, the nanocomposites specimens were oven dried and the ensuing weights demonstrated a 0.5% weight-loss. Therefore, any polymer loss should be at a maximum of 0.5%, which clearly indicates that the leaching of the cross-linked PMETAC from the BNC network is minimal.

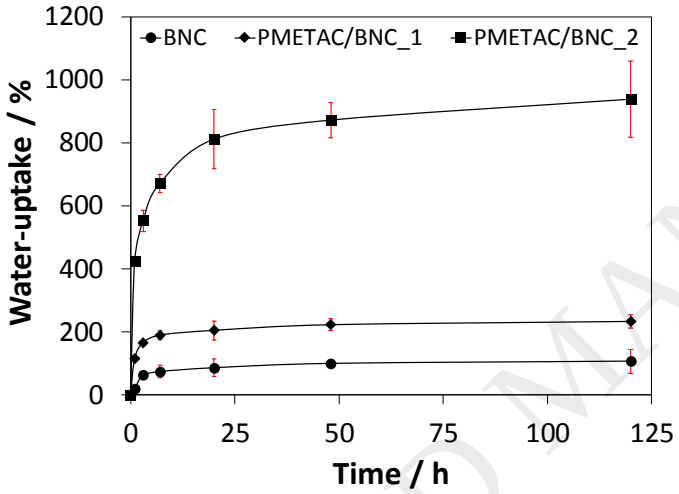

Fig. 5. Water-uptake as a function of time (0, 1, 3, 7, 20, 48 and 120 h) for BNC and nanocomposites PMETAC/BNC_1 and PMETAC/BNC_2 when immersed in water at room temperature; the values are the mean of three replicates and the error bars correspond to the standard deviations, and the lines are for visual guidance.

3.4. Thermal stability

The thermal degradation profile of the nanocomposites was evaluated by TGA analysis in order to get a deeper insight into their thermal stability. The TGA trace of the cross-linked PMETAC indicates a weight-loss degradation profile via two consecutive stages with maximum decomposition temperatures at 279 °C (T_{dmax1}) and

407 °C (T_{dmax2}, Table 2), due to the decomposition of quaternary ammonium groups that commonly takes place through Hofmann elimination reactions (Isik et al., 2013; Qi et al., 2017; Vilela, Sousa, et al., 2017). In turn, the trace of BNC exhibits a single-step degradation profile with a maximum decomposition temperature at 349 °C (T_{dmax}, Table 2) associated with the pyrolysis of the cellulose skeleton (Wang, Liu, Luo, Wen, & Cen, 2007).

Regarding the nanocomposites, the TGA analysis revealed a similar profile between the two nanocomposites regardless of the amount of cross-linked PMETAC incorporated into the BNC network. The two-step degradation profile of the nanocomposites, apart from the dehydration at *ca*. 100 °C, is attributed firstly (T_{dmax1}) to the degradation of pendant quaternary ammonium groups on the polymer backbone and the cellulose skeleton, and secondly (T_{dmax2}) to the degradation of the polymer backbone (Goel et al., 2009). A final residue of around 16% was obtained at temperatures up to 800 °C for both nanocomposites (Table 2), which corresponds to a total weight-loss value of 83–84%. Worth noting is the fact that a thermal stability up to 200 °C qualifies these nanocomposites for sterilization under typical procedures at *ca*. 150 °C (*e.g*. autoclaving), which is an essential requirement for most biomedical applications.

Table 2 TGA data of the cross-linked PMETAC, pure BNC and PMETAC/BNC nanocomposites.

Sample	T_{di}/°C	T_{dmax1}/°C	T_{dmax2}/°C	**Final residue/%**
PMETAC	200±0.5	279±0.6	407±0.9	4.5±1.2
BNC	265±0.7	349±0.8	–	13.1±0.5
PMETAC/BNC_1	210±0.5	266±0.5	380±0.5	16.6±0.2
PMETAC/BNC_2	210±0.4	260±0.5	395±0.4	16.1±0.6

3.5. Mechanical and viscoelastic properties

The mechanical performance of the PMETAC/BNC nanocomposites was determined from the corresponding stress-strain curves at room temperature. These properties were not evaluated for the cross-linked PMETAC owing to the lack of film-forming aptitude of this polymer. According to Fig. 6A, the Young's modulus, tensile strength and elongation at break obtained for the nanocomposites increased with the growing content of BNC (60 and 90 wt.%), because of the exceptional mechanical properties of this bacterial polysaccharide, namely the Young's modulus of 14.8±0.5 GPa, tensile strength of 221±4 MPa, and elongation at break of 2.4±0.2%, compatible with values reported in literature (Cacicedo et al., 2016). In fact, the Young's modulus of the nanocomposites increased from 2.4±0.4 GPa for PMETAC/BNC_2 (60 wt.% BNC) to 9.7±0.5 GPa for PMETAC/BNC_1 (90 wt.% BNC), and the same tendency is patent on the tensile strength that increases from 37±5 MPa for PMETAC/BNC_2 to 187±8 MPa for PMETAC/BNC_1 (Fig. 6A, $p<0.05$). Hence, the augment from 209±9 mg of PMETAC to 570±12 mg of PMETAC *per* cm^3 of nanocomposite points out the dependence of the nanocomposites' mechanical performance on the amount of BNC. This behaviour is in line with previous studies dealing with other BNC-based nanocomposites (Figueiredo, Figueiredo, et al., 2015; Vilela, Gadim, Silvestre, Freire, & Figueiredo, 2016). Furthermore, the Young's modulus and tensile strength of the PMETAC/BNC nanocomposites are superior to those described, for example, for the poly(lactic acid)/carvacrol electrospun membranes with antifungal activity against *C. albicans* (Scaffaro, Lopresti, D'Arrigo, Marino, & Nostro, 2018).

In the case of the elongation at break, the behaviour is different because the incorporation of 10 or 40 wt.% of cross-linked PMETAC into the BNC nanofibrous network did not have a significant effect on this parameter (Fig. 6A), given that the

means difference is not significant (α=0.05). These results reveal that, despite the lower Young's modulus and tensile strength values, the nanocomposites are still stiff with small values of elongation at break (PMETAC/BNC_1: 3.0±0.9% and PMETAC/BNC_2: 2.5±0.8%) just like BNC (2.4±0.2%). From the mechanical point of view, both nanocomposites are sufficiently pliable and workable (see Fig. 6B) for cutaneous applications dealing with the adhesion to irregular skin surfaces.

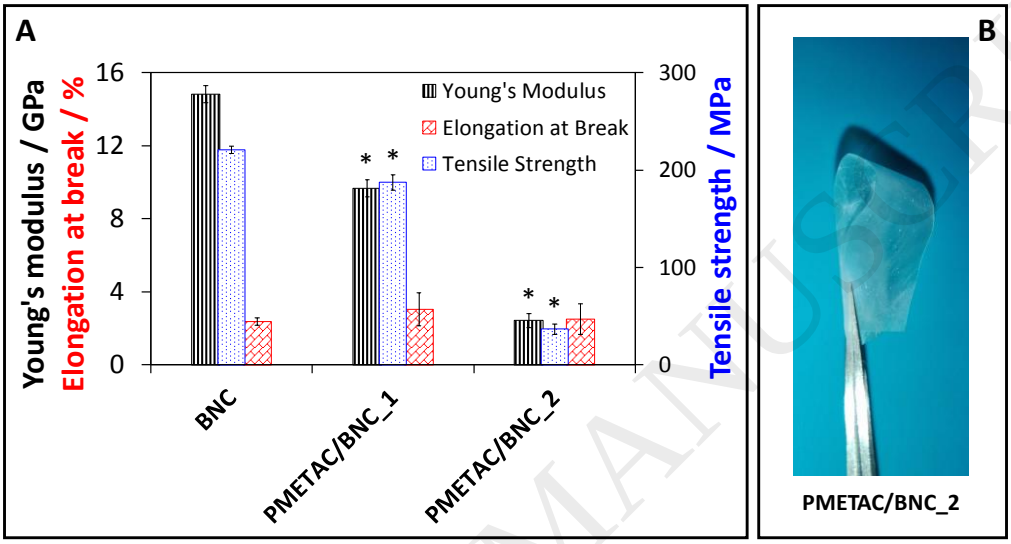

Fig. 6. (A) Young's modulus, tensile strength and elongation at break of pure BNC and PMETAC/BNC nanocomposites; the values are the mean of five replicates and the error bars correspond to the standard deviations; the asterisk (*) denotes statistically significant differences to the pure BNC ($p < 0.05$) and (B) photograph showing the bendable nanocomposite PMETAC/BNC_2.

The viscoelastic properties the PMETAC/BNC nanocomposites were measured by DMA and the storage modulus (E') and loss factor (tan δ) data is plotted in Fig. 7. Once again, the lack of film-forming aptitude of the cross-linked PMETAC hindered its analysis. Concerning the pristine BNC, the variation of E' with temperature has virtually no oscillations, being fairly stable up to at least 180 °C, as discussed elsewhere (Gadim et al., 2014). In the case of the nanocomposites, the story is different with

PMETAC/BNC_1 showing better viscoelastic properties than PMETAC/BNC_2 (Fig. 7) for the entire temperature range. Nanocomposite PMETAC/BNC_1 displays a reduction in *E*' from 9.7 GPa at −30 °C to 5.4 GPa at 88 °C, followed by a small increase to 6.3 GPa at 125 °C, and then another decrease to 4.9G at 180 °C. PMETAC/BNC_2 presents a pattern with smaller values where *E*' decreases from 3.9 GPa at −30 °C to 1.7 GPa at 45 °C, then increases to 3.1 GPa at 140 °C and slightly decreases to 2.9 GPa at 180 °C. Even though the *E*' drops to values of *ca*. 1.7 GPa at around 45 °C, the PMETAC/BNC_2 nanocomposite still preserves a satisfactory mechanical integrity endued by BNC, as already shown for other BNC-based nanocomposites (Gadim et al., 2014, 2016; Vilela et al., 2016). Furthermore, these results agree with the data from the mechanical tests outlined in Fig. 6A.

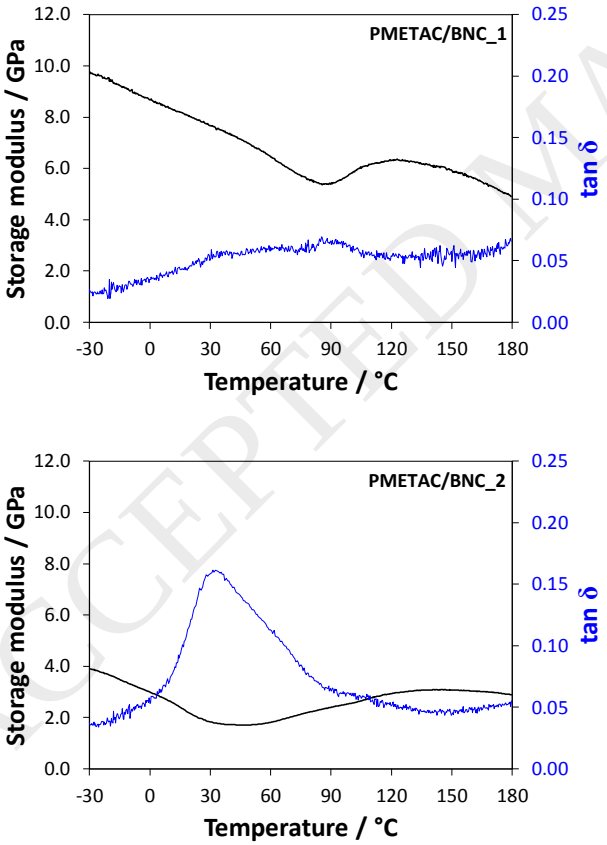

Fig. 7. Storage modulus and loss factor (tan *δ*) curves of PMETAC/BNC_1 and PMETAC/BNC_2 nanocomposites.

The loss factor (tan δ) validates the temperature dependence of the storage modulus with PMEATC/BNC_1 showing no relevant features and PMETAC/BNC_2 presenting a broad peak in the range 0 to 90 °C, as displayed in Fig. 7. The absence of any variation in the loss factor of PMETAC/BNC_1 reflects the high content of BNC (*i.e*. 90 wt.%), whereas the broad tan δ peak with maximum at *ca*. 32 °C might relate to the plasticizing effect of water on the PMETAC/BNC_2 nanocomposite due to the hygroscopic nature of PMETAC.

3.6. In vitro antifungal activity

The presence of quaternary ammonium groups in the chemical structure of the cross-linked PMETAC is expected to convert the nanocomposites into potential antifungal agents. Fig. 8 presents the antifungal activity of PMETAC/BNC nanocomposites together with that of pure BNC for comparison purposes. The experimental control was produced via inoculation of the fungus in culture media in the absence of sample. As expected, BNC has no effect on the fungal viability, showing an analogous behaviour to the control sample since BNC is deprived of antifungal activity or any other antimicrobial activity. In fact, BNC does not inhibit the growth of many microorganisms (*e.g*., *Escherichia coli* (Figueiredo, Figueiredo, et al., 2015; Padrão et al., 2016; Shao et al., 2016), *Staphylococcus aureus* (Padrão et al., 2016; Shao et al., 2016), *Pseudomonas aeruginosa*, *Bacillus subtilis* and *C. albicans* (Shao et al., 2016)) and can even be used as a substrate for microbial cell culture (Yin et al., 2014).

In the case of the studied nanocomposites, both inhibited the growth of *C. albicans* with 48 h of contact time, but the concentration of cross-linked PMETAC is the major factor affecting the growth inhibition. PMETAC/BNC_1 reached a 3.4±0.07–log reduction after 24 h and a maximum of 4.4±0.14–log reduction after 48 h, whereas the

highest growth inhibition was observed for the nanocomposite PMETAC/BNC_2 containing the highest content of cross-linked PMETAC with about 4.6±0.13–log reduction after 24 h and 5.5±0.19–log reduction after 48 h of incubation (Fig. 8). Clearly, these nanocomposites can be termed antifungal since they exhibit a minimum 3–log CFU reduction that is indicative of a killing efficiency higher than 99.9%. Shiga *et al*. verified that PMETAC has a MIC of 0.37 mg mL^{-1} (Shiga et al., 2018), and the nanocomposite with the lower PMETAC content (PMETAC/BNC_1) presents fungicidal activity at a concentration of 0.5 mg mL^{-1}. When compared with other systems, PMETAC/BNC nanocomposites present a comparable growth inhibition of fungal cells with, for example, the non-cytotoxic tissue conditioners based on poly(acryloyloxyethyltrimethyl ammonium chloride)–grafted chitosan (Lee et al., 2018).

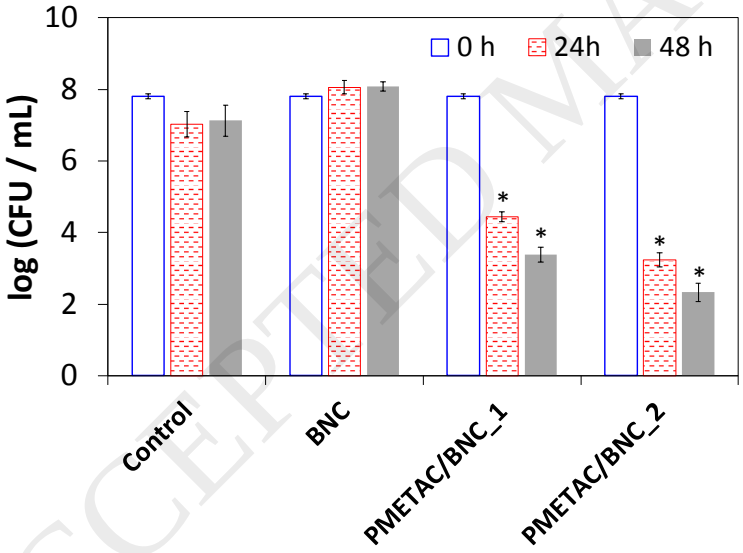

Fig. 8. Antifungal activity of BNC and nanocomposites PMETAC/BNC_1 and PMETAC/BNC_2 after 0, 24 and 48 h. Values represent the mean of three independent experiments; error bars represent the standard deviations; the asterisk (*) denotes statistically significant differences to the control and pure BNC ($p < 0.05$).

3.7. In vitro cytotoxicity assay

The cytotoxicity of the PMETAC/BNC nanocomposites was assessed in HaCaT cells through the indirect MTT assay (Mosmann, 1983). The metabolic activity of the HaCaT cells was normal for the negative control, *viz.* 100% cell viability (Fig. 9). BNC was non-cytotoxic to HaCaT cells for the exposure time, as already reported in literature for the same cells (Saïdi et al., 2017) and other cell lines (Figueiredo et al., 2013). This was expected given the recognised biocompatibility of BNC as discussed elsewhere (Silvestre et al., 2014; Sulaeva, Henniges, Rosenau, & Potthast, 2015).

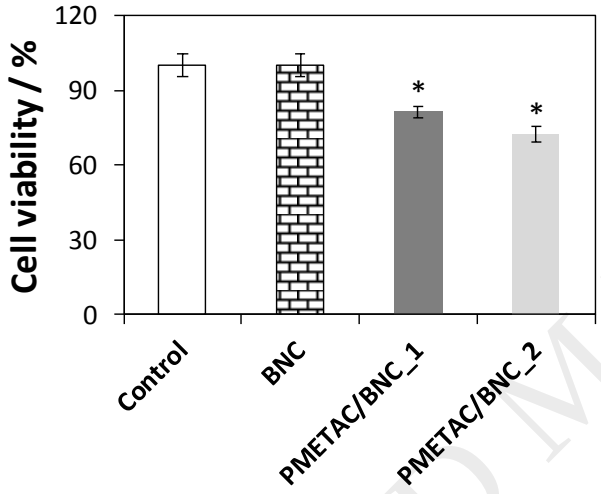

Fig. 9. Cell viability of HaCaT cells after exposure to negative control, BNC, PMETAC/BNC_1 and PMETAC/BNC_2 on the HaCaT cells for exposure time of 24 h. Values represent the mean of six replicates; error bars represent the standard deviation; the asterisk (*) denotes statistically significant differences to the control and pure BNC ($p < 0.05$).

The HaCaT cells cultured with different extracts of PMETAC/BNC nanocomposites showed a PMETAC content-dependent cell viability (Fig. 9, $p<0.05$). In fact, the cell viability of PMETAC/BNC_1 that contains 10 wt.% of cross-linked PMETAC was reduced to 81.4±2.1%, whereas for PMETAC/BNC_2 with 40 wt.% of

cross-linked PMETAC the cell viability decreased to 72.4±3.1%. Nevertheless, both nanocomposites are considered non-cytotoxic under these conditions since the cell viability was not reduced by more than 30% (ISO 10993-5:2009(E), 2009). These results agree with the non-cytotoxicity of PMETAC reported for BJ (CRL2522) (Mishra, Ramasamy, Ahmad, Eshak, & Majeed, 2014) and HeLa (Wang et al., 2018) cell lines.

The beauty of these PMETAC/BNC nanocomposites lies in the combination between the antifungal activity against *C. albicans* and their customizable properties depending on the amount of the individual components, namely the UV-blocking properties, water-uptake capacity, thermal stability, mechanical performance and non-cytotoxicity. Under these premises, we anticipate the application of these bioactive nanocomposites as potentially effective systems for the treatment of *C. albicans* cutaneous infections or even for application in medical devices requiring biocides to reduce fungal adhesion and biofilm formation such as catheters and prostheses.

4. Conclusions

The exploitation of the bioactive cationic poly([2–(methacryloyloxy)ethyl] trimethylammonium chloride) and the hydrophilic bacterial nanocellulose generated nanocomposites capable of inactivating the polymorphic fungus *C. albicans*. This one-pot strategy originated optically transparent PMETAC/BNC nanocomposites containing 209±9 and 570±12 mg of PMETAC *per* cm^3 of nanocomposite. Besides, these cationic nanocomposites exhibit UV–A and UV–B blocking properties, high water-uptake capacity, thermal stability up to 200 °C, along with good viscoelastic properties (storage modulus > 1.7 GPa) and mechanical performance (Young's modulus ≥ 2.4 GPa). The *in vitro* cytotoxicity assay showed that the nanocomposites are non-cytotoxic toward

HaCaT cells. Furthermore, their antifungal activity was demonstrated by the fungal inactivation of *C. albicans* that registered a 4.4±0.14–log reduction for the nanocomposite containing only 10 wt.% of PMETAC after 48 h. Hence, these customizable nanocomposites might show potential as bioactive systems to address the intricate issue of fungal infections, where antifungal materials play a key role in reducing/avoiding these types of ailments.

Acknowledgments

This work was developed within the scope of the projects CICECO-Aveiro Institute of Materials, FCT Ref. UID/CTM/50011/2019, and CESAM, FCT ref. UID/AMB/50017/2019, financed by national funds through the FCT/MEC. The research contracts of C. Vilela and H. Oliveira are funded by national funds (OE), through FCT – Fundação para a Ciência e a Tecnologia, I.P., in the scope of the framework contract foreseen in the numbers 4, 5 and 6 of article 23, of the Decree-Law 57/2016, of August 29, changed by Law 57/2017, of July 19. FCT is also acknowledged for the research contract under Stimulus of Scientific Employment 2017 to C.S.R. Freire (CEECIND/00464/2017).

References

Bellamy, L. J. (1975). *The infrared spectra of complex molecules* (3rd ed.). London: Chapman and Hall, Ltd.

Cacicedo, M. L., Castro, M. C., Servetas, I., Bosnea, L., Boura, K., Tsafrakidou, P., Dima, A., Terpou, A., Koutinas, A., & Castro, G. R. (2016). Progress in bacterial cellulose matrices for biotechnological applications. *Bioresource Technology*, *213*, 172–180. https://doi.org/10.1016/j.biortech.2016.02.071

Cielecka, I., Szustak, M., Gendaszewska-Darmach, E., Kalinowska, H., Ryngajłło, M., Maniukiewicz, W., & Bielecki, S. (2018). Novel bionanocellulose/κ-carrageenan composites for tissue engineering. *Applied Sciences*, *8*(8), 1352. https://doi.org/10.3390/app8081352

Dadar, M., Tiwari, R., Karthik, K., Chakraborty, S., Shahali, Y., & Dhama, K. (2018). Candida albicans - Biology, molecular characterization, pathogenicity, and advances in diagnosis and control – An update. *Microbial Pathogenesis*, *117*, 128–138. https://doi.org/10.1016/j.micpath.2018.02.028

De Prijck, K., De Smet, N., Coenye, T., Schacht, E., & Nelis, H. J. (2010). Prevention of Candida albicans biofilm formation by covalently bound dimethylaminoethylmethacrylate and polyethylenimine. *Mycopathologia*, *170*(4), 213–221. https://doi.org/10.1007/s11046-010-9316-3

Faria, M., Vilela, C., Mohammadkazemi, F., Silvestre, A. J. D., Freire, C. S. R., & Cordeiro, N. (2019). Poly(glycidyl methacrylate)/bacterial cellulose nanocomposites: Preparation, characterization and post-modification. *International Journal of Biological Macromolecules*, *127*, 618–627. https://doi.org/10.1016/j.ijbiomac.2019.01.133

Faria, M., Vilela, C., Silvestre, A. J. D., Deepa, B., Resnik, M., Freire, C. S. R., &

Cordeiro, N. (2019). Physicochemical surface properties of bacterial cellulose/polymethacrylate nanocomposites: an approach by inverse gas chromatography. *Carbohydrate Polymers*, *206*, 86–93. https://doi.org/10.1016/j.carbpol.2018.10.110

Fefelova, N. A., Nurkeeva, Z. S., Mun, G. A., & Khutoryanskiy, V. V. (2007). Mucoadhesive interactions of amphiphilic cationic copolymers based on [2-(methacryloyloxy)ethyl]trimethylammonium chloride. *International Journal of Pharmaceutics*, *339*(1–2), 25–32. https://doi.org/10.1016/j.ijpharm.2007.02.019

Figueiredo, A. G. P. R., Figueiredo, A. R. P., Alonso-Varona, A., Fernandes, S. C. M., Palomares, T., Rubio-Azpeitia, E., Barros-Timmons, A., Silvestre, A. J. D., Neto, C. P., & Freire, C. S. R. (2013). Biocompatible bacterial cellulose-poly(2-hydroxyethyl methacrylate) nanocomposite films. *BioMed Research International*, *698141*, 1–14. https://doi.org/10.1155/2013/698141

Figueiredo, A. R. P., Figueiredo, A. G. P. R., Silva, N. H. C. S., Barros-Timmons, A., Almeida, A., Silvestre, A. J. D., & Freire, C. S. R. (2015). Antimicrobial bacterial cellulose nanocomposites prepared by in situ polymerization of 2-aminoethyl methacrylate. *Carbohydrate Polymers*, *123*, 443–453. https://doi.org/10.1016/j.carbpol.2015.01.063

Figueiredo, A. R. P., Vilela, C., Neto, C. P., Silvestre, A. J. D., & Freire, C. S. R. (2015). Bacterial cellulose-based nanocomposites: Roadmap for innovative materials. In V. K. Thakur (Ed.), *Nanocellulose polymer composites* (pp. 17–64). Scrivener Publishing LLC. https://doi.org/10.1002/9781118872246.ch2

Gadim, T. D. O., Figueiredo, A. G. P. R., Rosero-Navarro, N. C., Vilela, C., Gamelas, J. A. F., Barros-Timmons, A., Neto, C. P., Silvestre, A. J. D., Freire, S. R., & Figueiredo, F. M. L. (2014). Nanostructured bacterial cellulose-poly(4-styrene

sulfonic acid) composite membranes with high storage modulus and protonic conductivity. *ACS Applied Materials & Interfaces*, *6*(10), 7864–7875. https://doi.org/10.1021/am501191t

Gadim, T. D. O., Vilela, C., Loureiro, F. J. A., Silvestre, A. J. D., Freire, C. S. R., & Figueiredo, F. M. L. (2016). Nafion® and nanocellulose: a partnership for greener polymer electrolyte membranes. *Industrial Crops and Products*, *93*, 212–218. https://doi.org/10.1016/j.indcrop.2016.01.028

Gama, M., Dourado, F., & Bielecki, S. (2017). *Bacterial nanocellulose : from biotechnology to bio-economy*. Elsevier.

Goel, N. K., Rao, M. S., Kumar, V., Bhardwaj, Y. K., Chaudhari, C. V., Dubey, K. A., & Sabharwal, S. (2009). Synthesis of antibacterial cotton fabric by radiation-induced grafting of [2-(methacryloyloxy)ethyl]trimethylammonium chloride (MAETC) onto cotton. *Radiation Physics and Chemistry*, *78*(6), 399–406. https://doi.org/10.1016/j.radphyschem.2009.03.011

Greca, L. G., Lehtonen, J., Tardy, B. L., Guo, J., & Rojas, O. J. (2018). Biofabrication of multifunctional nanocellulosic 3D structures: a facile and customizable route. *Materials Horizons*, *5*, 408–415. https://doi.org/10.1039/C7MH01139C

Gupta, A., Avci, P., Dai, T., Huang, Y.-Y., & Hamblin, M. R. (2013). Ultraviolet radiation in wound care: sterilization and stimulation. *Advances in Wound Care*, *2*(8), 422–437. https://doi.org/10.1089/wound.2012.0366

Isik, M., Gracia, R., Kollnus, L. C., Tomé, L. C., Marrucho, I. M., & Mecerreyes, D. (2013). Cholinium-based poly(ionic liquid)s: Synthesis, characterization, and application as biocompatible ion gels and cellulose coatings. *ACS Macro Letters*, *2*(11), 975–979. https://doi.org/10.1021/mz400451g

ISO 10993-5:2009(E). (2009). Biological evaluation of medical devices - Part 5: Tests

for in vitro cytotoxicity.

Kühbacher, A., Burger-Kentischer, A., & Rupp, S. (2017). Interaction of Candida species with the skin. *Microorganisms, 5*, 32. https://doi.org/10.3390/microorganisms5020032

Lee, H.-L., Wang, R.-S., Hsu, Y.-C., Chuang, C.-C., Chan, H.-R., Chiu, H.-C., Wang, Y.-B., Chen, K.-Y., & Fu, E. (2018). Antifungal effect of tissue conditioners containing poly(acryloyloxyethyltrimethyl ammonium chloride)-grafted chitosan on Candida albicans growth in vitro. *Journal of Dental Sciences*, *13*(2), 160–166. https://doi.org/10.1016/J.JDS.2017.06.004

Li, J., Cha, R., Mou, K., Zhao, X., Long, K., Luo, H., Zhou, F., & Jiang, X. (2018). Nanocellulose-based antibacterial materials. *Advanced Healthcare Materials*, *7*, 1800334. https://doi.org/10.1002/adhm.201800334

Mayer, F. L., Wilson, D., & Hube, B. (2013). Candida albicans pathogenicity mechanisms. *Virulence*, *4*(2), 119–128. https://doi.org/10.4161/viru.22913

Mishra, R. K., Ramasamy, K., Ahmad, N. A., Eshak, Z., & Majeed, A. B. A. (2014). pH dependent poly[2-(methacryloyloxyethyl)trimetylammonium chloride-co-methacrylic acid]hydrogels for enhanced targeted delivery of 5-fluorouracil in colon cancer cells. *Journal of Materials Science: Materials in Medicine*, *25*(4), 999–1012. https://doi.org/10.1007/s10856-013-5132-x

Morales, D. V., Rivas, B. L., & Escalona, N. (2016). Poly([(2-methacryloyloxy)ethyl] trimethylammonium chloride): synthesis, characterization, and removal properties of As(V). *Polymer Bulletin*, *73*(3), 875–890. https://doi.org/10.1007/s00289-015-1524-z

Morales, D. V., Rivas, B. L., & González, M. (2016). Synthesis and characterization of poly([(2-methacryloyloxy) ethyl]) trimethylamonnium chloride) resin with

removal properties for vanadium(V) and molybdenum(VI). *Journal of the Chilean Chemical Society*, *61*(4), 3295–3303. https://doi.org/10.4067/S0717-97072016000400029

Mosmann, T. (1983). Rapid colorimetric assay for cellular growth and survival: application to proliferation and cytotoxicity assays. *Journal of Immunological Methods*, *65*(1–2), 55–63. https://doi.org/10.1016/0022-1759(83)90303-4

Muñoz-Bonilla, A., & Fernández-García, M. (2018). Poly(ionic liquid)s as antimicrobial materials. *European Polymer Journal*, *105*, 135–149. https://doi.org/10.1016/j.eurpolymj.2018.05.027

Nurkeeva, Z. S., Mun, G. A., Sergaziyev, A. D., Fefelova, N. A., Sarsenbaeva, A. S., & Khutoryanskiy, V. V. (2006). Synthesis of cationic water-soluble copolymers and hydrogels based on [2-(methacryloyloxy)ethyl]trimethylammonium chloride and 2-hydroxyethylacrylate and their complex formation with poly(acrylic acid). *Journal of Polymer Science Part B: Polymer Physics*, *44*(5), 845–853. https://doi.org/10.1002/polb.20742

Padrão, J., Gonçalves, S., Silva, J. P., Sencadas, V., Lanceros-Méndez, S., Pinheiro, A. C., Vicente, A. A., Rodrigues, L. R., & Dourado, F. (2016). Bacterial cellulose-lactoferrin as an antimicrobial edible packaging. *Food Hydrocolloids*, *58*, 126–140. https://doi.org/10.1016/j.foodhyd.2016.02.019

Pinto, E. R. P., Barud, H. S., Silva, R. R., Palmieri, M., Polito, W. L., Calil, V. L., Cremona, M., Ribeiro, S. J. L., & Messaddeq, Y. (2015). Transparent composites prepared from bacterial cellulose and castor oil based polyurethane as substrates for flexible OLEDs. *Journal of Materials Chemistry C*, *3*(44), 11581–11588. https://doi.org/10.1039/c5tc02359a

Qi, X., Li, J., Wei, W., Zuo, G., Su, T., Pan, X., Zhang, J., & Dong, W. (2017). Cationic

Salecan-based hydrogels for release of 5-fluorouracil. *RSC Advances*, *7*(24), 14337–14347. https://doi.org/10.1039/c7ra01052d

Ray, D., & Sain, S. (2016). In situ processing of cellulose nanocomposites. *Composites Part A: Applied Science and Manufacturing*, *83*, 19–37. https://doi.org/10.1016/j.compositesa.2015.09.007

Saïdi, L., Vilela, C., Oliveira, H., Silvestre, A. J. D., & Freire, C. S. R. (2017). Poly(N-methacryloyl glycine)/nanocellulose composites as pH-sensitive systems for controlled release of diclofenac. *Carbohydrate Polymers*, *169*, 357–365. https://doi.org/10.1016/j.carbpol.2017.04.030

Scaffaro, R., Lopresti, F., D'Arrigo, M., Marino, A., & Nostro, A. (2018). Efficacy of poly(lactic acid)/carvacrol electrospun membranes against Staphylococcus aureus and Candida albicans in single and mixed cultures. *Applied Microbiology and Biotechnology*, *102*(9), 4171–4181. https://doi.org/10.1007/s00253-018-8879-7

Shao, W., Wang, S., Wu, J., Huang, M., Liu, H., & Min, H. (2016). Synthesis and antimicrobial activity of copper nanoparticle loaded regenerated bacterial cellulose membranes. *RSC Advances*, *6*(70), 65879–65884. https://doi.org/10.1039/c6ra07984a

Sheppard, D. C., & Howell, P. L. (2016). Biofilm exopolysaccharides of pathogenic fungi: Lessons from bacteria. *Journal of Biological Chemistry*, *291*(24), 12529–12537. https://doi.org/10.1074/jbc.R116.720995

Shiga, T., Mori, H., Uemura, K., Moriuchi, R., Dohra, H., Yamawaki-Ogata, A., Narita, Y., Saito, A., & Kotsuchibashi, Y. (2018). Evaluation of the bactericidal and fungicidal activities of poly([2-(methacryloyloxy)ethyl]trimethyl ammonium chloride)(poly (METAC))-based materials. *Polymers*, *10*(9), 947. https://doi.org/10.3390/polym10090947

Silva, N. H. C. S., Vilela, C., Almeida, A., Marrucho, I. M., & Freire, C. S. R. (2018). Pullulan-based nanocomposite films for functional food packaging: exploiting lysozyme nanofibers as antibacterial and antioxidant reinforcing additives. *Food Hydrocolloids*, *77*, 921–930. https://doi.org/10.1016/j.foodhyd.2017.11.039

Silva, N. H. C. S., Vilela, C., Marrucho, I. M., Freire, C. S. R., Pascoal Neto, C., & Silvestre, A. J. D. (2014). Protein-based materials: from sources to innovative sustainable materials for biomedical applications. *Journal of Materials Chemistry B*, *2*(24), 3715–3740. https://doi.org/10.1039/c4tb00168k

Silvestre, A. J. D., Freire, C. S. R., & Neto, C. P. (2014). Do bacterial cellulose membranes have potential in drug-delivery systems? *Expert Opinion on Drug Delivery*, *11*(7), 1113–1124. https://doi.org/10.1517/17425247.2014.920819

Soll, D. R., & Daniels, K. J. (2016). Plasticity of Candida albicans biofilms. *Microbiology and Molecular Biology Reviews*, *80*(3), 565–595. https://doi.org/10.1128/mmbr.00068-15

Stopiglia, C. D. O., Collares, F. M., Ogliari, F. A., Piva, E., Fortes, C. B. B., Samuel, S. M. W., & Scroferneker, M. L. (2012). Antimicrobial activity of [2-(methacryloyloxy)ethyl]trimethylammonium chloride against Candida spp. *Revista Iberoamericana de Micología*, *29*(1), 20–23. https://doi.org/10.1016/j.riam.2011.03.003

Subtaweesin, C., Woraharn, W., Taokaew, S., Chiaoprakobkij, N., Sereemaspun, A., & Phisalaphong, M. (2018). Characteristics of curcumin-loaded bacterial cellulose films and anticancer properties against malignant melanoma skin cancer cells. *Applied Sciences*, *8*(7), 1188. https://doi.org/10.3390/app8071188

Sulaeva, I., Henniges, U., Rosenau, T., & Potthast, A. (2015). Bacterial cellulose as a material for wound treatment: Properties and modifications: A review.

Biotechnology Advances, *33*(8), 1547–1571. https://doi.org/10.1016/j.biotechadv.2015.07.009

Trovatti, E., Serafim, L. S., Freire, C. S. R., Silvestre, A. J. D., & Neto, C. P. (2011). Gluconacetobacter sacchari: An efficient bacterial cellulose cell-factory. *Carbohydrate Polymers*, *86*(3), 1417–1420. https://doi.org/10.1016/j.carbpol.2011.06.046

Tsui, C., Kong, E. F., & Jabra-Rizk, M. A. (2016). Pathogenesis of Candida albicans biofilm. *Pathogens and Disease*, *74*(4), ftw018. https://doi.org/10.1093/femspd/ftw018

Vilela, C., Gadim, T. D. O., Silvestre, A. J. D., Freire, C. S. R., & Figueiredo, F. M. L. (2016). Nanocellulose/poly(methacryloyloxyethyl phosphate) composites as proton separator materials. *Cellulose*, *23*(6), 3677–3689. https://doi.org/10.1007/s10570-016-1050-7

Vilela, C., Martins, A. P. C., Sousa, N., Silvestre, A. J. D., Figueiredo, F. M. L., & Freire, C. S. R. (2018). Poly(bis[2-(methacryloyloxy)ethyl] phosphate)/bacterial cellulose nanocomposites: Preparation, characterization and application as polymer electrolyte membranes. *Applied Sciences*, *8*(7), 1145. https://doi.org/10.3390/app8071145

Vilela, C., Pinto, R. J. B., Coelho, J., Domingues, M. R. M., Daina, S., Sadocco, P., Santos, S. A. O., & Freire, C. S. R. (2017). Bioactive chitosan/ellagic acid films with UV-light protection for active food packaging. *Food Hydrocolloids*, *73*, 120–128. https://doi.org/10.1016/j.foodhyd.2017.06.037

Vilela, C., Pinto, R. J. B., Figueiredo, A. R. P., Neto, C. P., Silvestre, A. J. D., & Freire, C. S. R. (2017). Development and applications of cellulose nanofibers based polymer composites. In E. Bafekrpour (Ed.), *Advanced Composite Materials:*

Properties and Applications (pp. 1–65). De Gruyter Open. https://doi.org/10.1515/9783110574432-001

Vilela, C., Pinto, R. J. B., Pinto, S., Marques, P. A. A. P., Silvestre, A. J. D., & Freire, C. S. R. (2018). *Polysaccharide based hybrid materials* (1st ed.). Springer. https://doi.org/10.1007/978-3-030-00347-0

Vilela, C., Sousa, N., Pinto, R. J. B., Silvestre, A. J. D., Figueiredo, F. M. L., & Freire, C. S. R. (2017). Exploiting poly(ionic liquids) and nanocellulose for the development of bio-based anion-exchange membranes. *Biomass and Bioenergy*, *100*, 116–125. https://doi.org/10.1016/j.biombioe.2017.03.016

Wang, H., Chen, M., Jin, C., Niu, B., Jiang, S., Li, X., & Jiang, S. (2018). Antibacterial [2-(methacryloyloxy) ethyl] trimethylammonium chloride functionalized reduced graphene oxide/poly(ethylene-co-vinyl alcohol) multilayer barrier film for food packaging. *Journal of Agricultural and Food Chemistry*, *66*(3), 732–739. https://doi.org/10.1021/acs.jafc.7b04784

Wang, J., & Vermerris, W. (2016). Antimicrobial nanomaterials derived from natural products-a review. *Materials*, *9*, 255. https://doi.org/10.3390/ma9040255

Wang, S., Liu, Q., Luo, Z., Wen, L., & Cen, K. (2007). Mechanism study on cellulose pyrolysis using thermogravimetric analysis coupled with infrared spectroscopy. *Frontiers of Energy and Power Engineering in China*, *1*(4), 413–419. https://doi.org/10.1007/s11708-007-0060-8

Yin, N., Santos, T. M. A., Auer, G. K., Crooks, J. A., Oliver, P. M., & Weibel, D. B. (2014). Bacterial cellulose as a substrate for microbial cell culture. *Applied and Environmental Microbiology*, *80*(6), 1926–32. https://doi.org/10.1128/aem.03452-13

Zida, A., Bamba, S., Yacouba, A., Ouedraogo-Traore, R., & Guiguemdé, R. T. (2017).

Anti-Candida albicans natural products, sources of new antifungal drugs: A review. *Journal de Mycologie Médicale*, *27*(1), 1–19. https://doi.org/10.1016/j.mycmed.2016.10.002